12th International Symposium on Turbulence and Shear Flow Phenomena (TSFP12)
Osaka, Japan (Online), July 19-22, 2022

ON LATE STAGES OF TRANSITION IN ROUND JETS

Naveen Balakrishna
Dept. of Aerospace Engg.
Indian Institute of Science
Bengaluru, India, 560012
naveenb@iisc.ac.in

Joseph Mathew
Dept. of Aerospace Engg.
Indian Institute of Science
Bengaluru, India, 560012
joseph@iisc.ac.in

Arnab Samanta
Dept. of Aerospace Engg.
Indian Institute of Technology
Kanpur, India, 208016
asamanta@iitk.ac.in

ABSTRACT

The bounding shear layer present near the nozzle exit of low-speed round jets undergoes Kelvin-Helmholtz instability that rolls up into vortex rings. These rings experience azimuthal instability and the ensuing nonlinear evolution sees the formation of secondary structures and the ejection of hairpin vortices into the wake of the ring. The importance of hairpin vortices in the laminar-turbulent transition process of round jets has received little attention, and this is a preliminary work in that direction. Using Direct Numerical Simulations (DNS), we study the evolution of an isolated hairpin vortex, modelled as a semi-ellipse with a Gaussian vorticity distribution in its core. The evolution is also explored in the presence of a uniformly convecting stream and a uniformly sheared background flow. The tip of the hairpin vortex moves up due to self-induction, while its legs approach each other upstream of the tip. This leads to a viscous vortex reconnection process leading to the pinch-off of ring-like vortices. Such reconnections of hairpin vortices, considered here, are qualitatively similar to those observed in other configurations, like antiparallel line vortices. As the Reynolds number increases, the time to reconnect decreases, while it occurs for increasingly smaller times. The presence of a uniformly convecting background flow has no effect on the reconnection process, while a uniform shear either accelerates or decelerates the process, depending upon the sense of this shear. This study shows hairpin vortex reconnection to be an important mechanism in the formation of small scales in the wake of vortex rings during a round jet transition.

INTRODUCTION

Round jets, common in many industrial applications and natural processes, are classified into laminar, transitional or turbulent, based on the nature of nozzle-exit boundary layer. An initially laminar jet usually transitions into a turbulent jet, which often involves multiple stages of several instability mechanisms. For example, the shear layer of a laminar jet is subjected to the classical Kelvin-Helmholtz instability (Michalke, 1984), which eventually rolls up into vortex rings via nonlinear mechanisms. Such vortex rings are subjected to two types of short-wavelength azimuthal instabilities: elliptic (Widnall & Tsai, 1977) and curvature (Fukumoto & Hattori, 2005), with the former being more commonly observed for rings during transition of round jets, which we study here. Elliptic instability leads to the formation of periodic waves around the circumference of vortex rings, whose period depends upon the ratio of core to ring radius and also on the details of vorticity distribution inside the core (Balakrishna *et al.*, 2020). Nonlinear evolution of these waves lead to the formation of complex secondary structures, referred to in the literature as “halo vorticity”and “inner core”, which eventually break down to initially form hairpin vortices and later other rings or ring-like structures, thereby completing the transition to turbulence (Archer *et al.*, 2008). Here, the number of azimuthal waves around the ring circumference determines the number of halo and hairpin vortices.

The formation of ring-like vortices in the late stages of transition from hairpin vortices were studied in the past using a localized induction approach and the Biot-Savart law by Hama (1962) and Moin *et al.* (1986), respectively. Both these studies included an isolated hairpin, modelled as a parabola, which due to its tip curvature has larger normal self-induced velocities there, thereby bringing in its legs closer together upstream of the tip, beyond which point these studies were stopped owing to worsening numerical accuracies. Additionally, Moin *et al.* (1986) also studied the Biot-Savart evolution of this isolated hairpin in the presence of a wall and uniform shear, and speculated that viscous vortex reconnection can occur when hairpin legs come closer, leading to the formation of ring-like vortices. However, such a vortex reconnection in hairpin vortices formed during a round jet transition is yet to be demonstrated, which we show in this work.

More recently, Biot-Savart evolution of antiparallel vortex rings has been studied, first in an ideal fluid by De Waele & Aarts (1994), who concluded that vortices form a pyramid structure at their closest approach point, independent of initial conditions. Hussain & Duraisamy (2011) in their DNS of antiparallel line vortices included the effect of viscosity at the closest approach point over a range of Reynolds numbers $Re = \Gamma/\nu$ (250-9000), where Γ and ν are circulation and kinematic viscosity, respectively. They observed a cascade of viscous vortex reconnection events, confirming the conclusions of Melander & Hussain (1988) that the viscous reconnection is not always completed at one go and that there are left over vortices that may undergo further reconnections at the smaller scales (see also Yao & Hussain, 2020*b*). Based on such observations, Moffatt & Kimura (2019*a*,*b*) proposed the pyramid model of viscous vortex reconnection, where two approaching vortices are set on two opposite faces of a pyramid that reconnect near the pyramid tip, thereafter moving downwards to complementary faces, while the surviving vortices move upwards to the tip for further reconnections.

In this work, to demonstrate the viscous vortex reconnections in hairpin structures, we use the isolated hairpin configuration of Moin *et al.* (1986), but allow for its viscous evolution via a DNS. Instead of a parabola, as taken by Moin *et al.* (1986), our isolated hairpin is a semi-ellipse with Gaussian vorticity distribution inside its core. Further, we also investigate the effect of uniformly convecting background streams and uniform background shears on this hairpin, which act here as simplified models for the presence of other vortical structures during a round jet transition process.

NUMERICAL METHODS

The initial velocity field is obtained from a Gaussian vorticity field by solving Poisson equations, with the latter as the source term. This vorticity field is specified inside the core of an ellipse of radius a, which is centrally-located on the $y = 0$ plane with an aspect ratio of AR $= a'/b' = 20$, where a' and b' are the lengths of the semi-major and semi-minor axis, respectively (see Fig. 1). The computational domain has dimensions of $0 < x < L_x$, $-L_y/4 < y < 3L_y/4$ and $-L_z/2 < z < L_z/2$, as shown in Fig. 1, with the length and time scales for the nondimensionalization being b' and b'^2/Γ, respectively. In this work, both the DNS and the solutions to Poisson equations are obtained via the open-source, incompressible Navier-Stokes solver, Incompact3D (Laizet & Lamballais, 2009; Laizet & Li, 2011).

In addition to the initial velocity field of the hairpin, we also study cases where a uniformly convecting background flow and a uniform background shear are added, to understand their roles in the hairpin evolution. A free-slip boundary condition is specified in the y direction when simulating these background flows, which are defined as $u_x(x, y, z) = Sy + U_c$, with U_c chosen based on the slope S such that the streamwise velocity u_x is non-zero at the lower boundary $y = -L_y/4$ (see Table 1 and Fig. 1). A Neumann condition is imposed at the $x = 0$ boundary by forcing the normal derivative of all the velocity components to zero, since it then allows the hairpin to move freely at the inflow end, which gets distorted otherwise due to its self-induced velocity and the background flow, if present. At $x = L_x$, convective boundary conditions are applied, while in the z direction, we use periodic boundary conditions. The length (same as that of Moin *et al.*, 1986) and position of the hairpin are chosen such that its tip evolution is unaffected by the boundaries. Further, an averaging operation is performed at each time step to preserve its initial symmetry about the $z = 0$ plane (see Fig. 1).

The grid resolution is chosen based on the conservation of volume-integrated kinetic energy (E_V) and the convergence of E_V and enstrophy (Ω). The maximum relative error between the left and right-hand sides of the kinetic energy conservation equation is less than 1.7% for the cases in Table 1, while the relative error for enstrophy and volume-integrated kinetic energy between the coarse (grid resolution of Table 1) and fine grid is $\approx 0.7\%$ and $\approx 0.3\%$, respectively (see Naveen, 2022, for convergence studies).

RESULTS

We first show the temporal evolution of azimuthal instability in an isolated vortex ring to demonstrate the occurrence of halo and hairpin-like vortices. This is shown in Fig. 2 at a few representative times, computed via Incompact3D following the procedure of Archer *et al.* (2008). Clearly, the formation of “halo vorticity”and their break down into a series of hairpin-like vortices can be seen in Figs. 2(b) and (c), respectively (see Naveen, 2022, for more details). Note that unlike in wall-bounded flows, here, such hairpin-like structures seem to coexist with a range of smaller scales so the latter may be presumed to have a role on the evolution of these hairpins, leading to the eventual ring breakdown. As a first step toward decoding such a breakdown, we study the evolution of an isolated hairpin vortex, also in the presence of either a uniformly convecting stream or a uniformly shearing flow. Using a quiescent flow, we first explore the effect of Reynolds number on the hairpin vortex evolution, followed by the background flows. Our simulations with quiescent flow are designated with the prefix $\mathrm{H_W}$, while the cases with a uniformly convecting stream and uniform shear have prefixes $\mathrm{H_U}$ and $\mathrm{H_S}$, respectively (see also Table 1).

Table 1. Cases used for the study of hairpin vortex evolution. The core radius is 0.3 for all the cases in this table.

Case	L_x	L_y	L_z	N_x	N_y	N_z	U_c	S	Re
$\mathrm{H_W}1$	25	20	10	641	513	256	0	0	3000
$\mathrm{H_W}2$	25	20	10	641	513	256	0	0	1500
$\mathrm{H_U}1$	35	20	10	897	513	256	0.2	0	1500
$\mathrm{H_U}2$	35	20	10	897	513	256	0.1	0	1500
$\mathrm{H_S}1$	35	20	10	897	513	256	0.2	0.01	1500
$\mathrm{H_S}2$	35	20	10	897	513	256	0.2	-0.01	1500

Effects of Reynolds number

The effects of Reynolds number on the hairpin evolution is explored in cases $\mathrm{H_W}1$ and $\mathrm{H_W}2$ of Table 1 and demonstrated in Figs. 3-5. In both the cases, the initial evolution of the hairpin tip is similar to the Biot-Savart evolution of Moin *et al.* (1986), where the entire hairpin shows an upward motion due to its self-induced velocity as its legs act as counter-rotating line vortices (compare the location of hairpin in (a) and (d) of Fig. 3). Additionally, the hairpin tip is raised above the plane of its legs due to an increased self-induced velocity caused by the small radius of curvature there. Later, with an increased radius of curvature it attains a circular shape, which brings the hairpin legs closer upstream (see Fig. 3b). The evolution of our hairpin beyond this point departs from the Biot-Savart evolution of hairpin line vortices, as studied by Moin *et al.* (1986), who were unable to continue their Biot-Savart evolution further due to worsening numerical accuracy. In spite of this, Moin *et al.* (1986) had speculated the occurrence of vortex reconnection as the viscous effects would start to dominate, splitting the initial hairpin into a secondary hairpin and vortex ring. Our DNS simulations clearly demonstrate this event of viscous vortex reconnection and the associated splitting of the initial hairpin vortex (see Figs. 3b-d).

In Fig. 4, a closer look of the reconnection process shows it to be almost identical to that in other configurations, e.g. antiparallel line vortices (see Yao & Hussain, 2020b), where the self-induced velocity brings the hairpin legs closer, upstream of its tip, leading to their collision. At the collision point, the vorticity in the adjacent legs gets annihilated due to viscosity which leads to the closest vortex lines from the legs to get cut and connect. Such connected vortex lines are next brought to the top, get stretched due to the induced velocities, eventually becoming perpendicular to the legs (see Melander & Hussain, 1988). With time, more such vortex lines are connected and brought to the top, thereby forming a perpendicular bridge (see Fig. 4a). This process continues until the bridges start to move away from each other due to their self-induced velocities, leaving the unreconnected vortex lines in the form of antiparallel sheet-like structures, called threads (see Fig. 4b). The

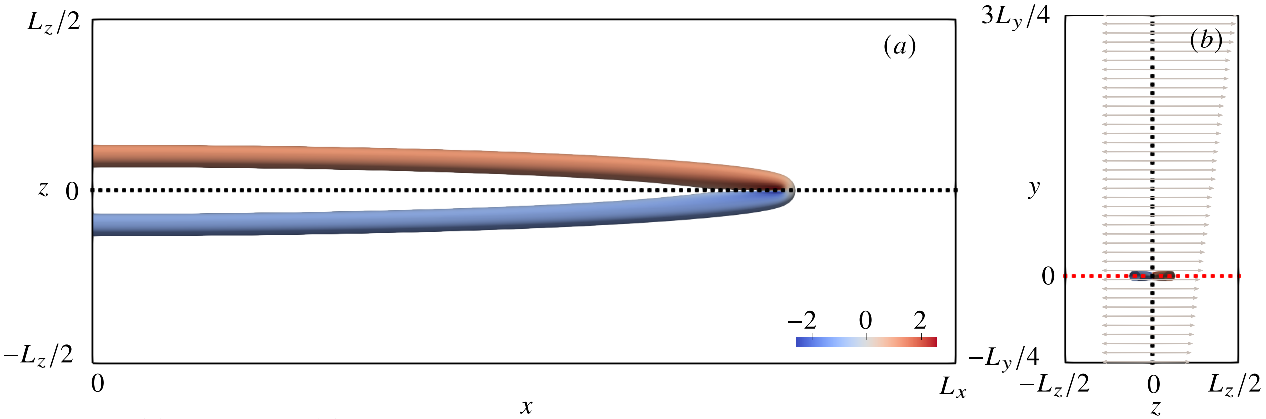

Figure 1. (a) Plan view and (b) end view showing the initial location of the hairpin vortex in the computational domain visualised with contour of $\lambda_2 = -0.1$ and coloured with axial vorticity (ω_x). The $z = 0$ and $y = 0$ planes are represented as ······and ······, respectively. The grey arrows in (b) indicate the background velocity field (u_x) for the cases $\mathrm{H_U}1$ ($z < 0$) and $\mathrm{H_S}1$ ($z > 0$).

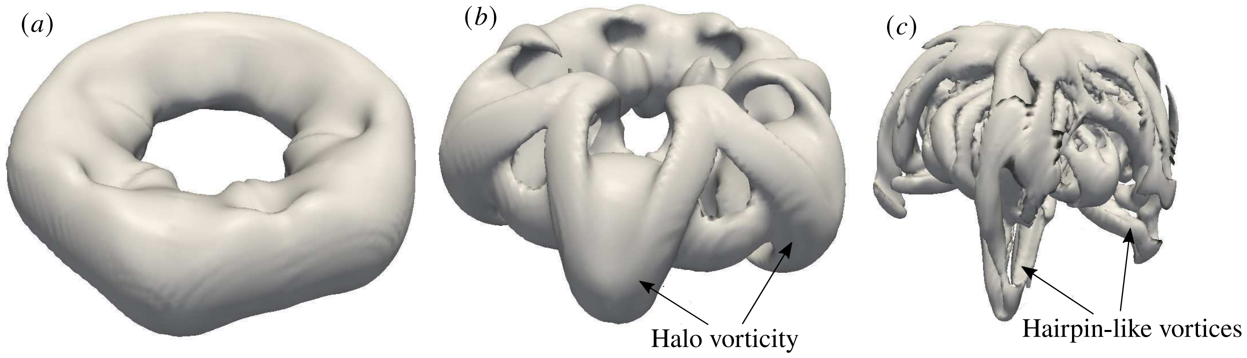

Figure 2. Evolution of vortex ring shown with contours of $\lambda_2 = -0.001$ at different times (a) t = 110; (b) t = 150; (c) t = 176.5.

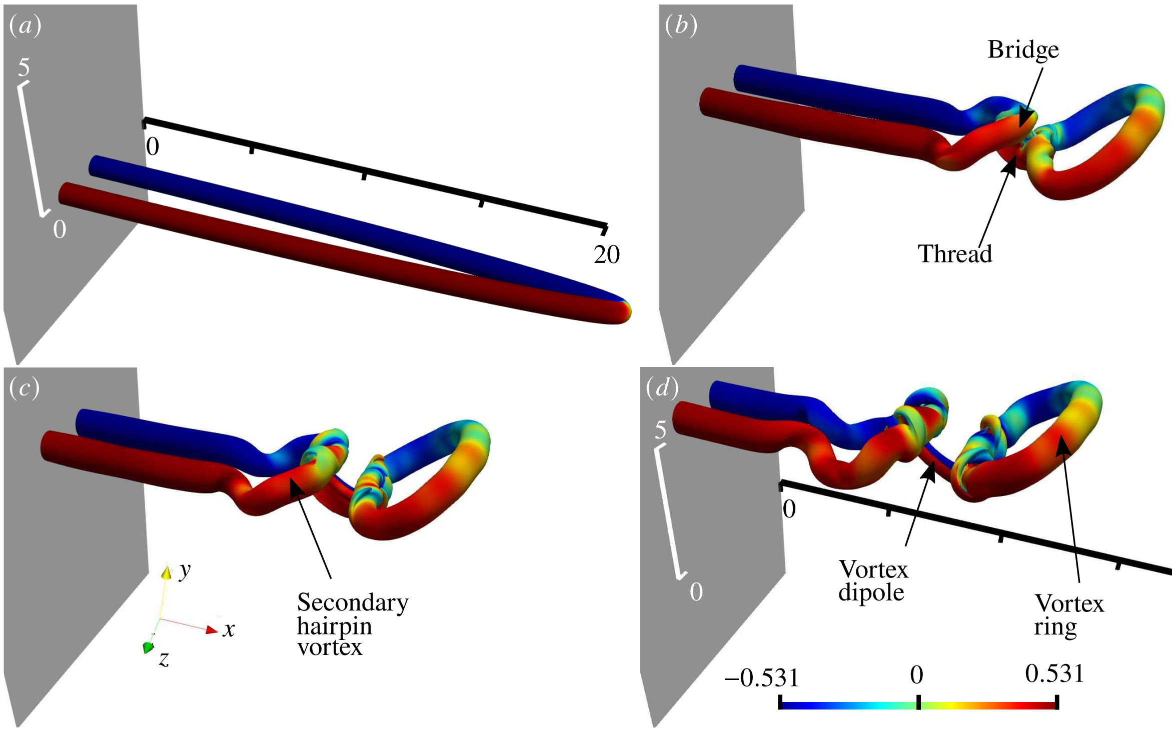

Figure 3. Isosurfaces of vorticity magnitude $|\boldsymbol{\omega}| = 0.15|\boldsymbol{\omega}|_0$ coloured with contours of ω_x for the case $\mathrm{H_W}1$ at $t = 0$ (a), $t = 55$ (b), $t = 65$ (c) and $t = 80$ (d). The inflow plane is coloured in grey and a part of axis is provided in (a) and (d) to show the upward motion of the hairpin vortex as the simulation proceeds from $t = 0$ (a) to $t = 80$ (d). Here, $|\boldsymbol{\omega}|_0$ is the maximum vorticity magnitude at $t = 0$.

induced velocity of the bridges between the threads is similar to a planar jet-like flow, which reverses the curvature of the threads and slows down their reconnection. At the same time, the mutual induction between these threads causes their peak

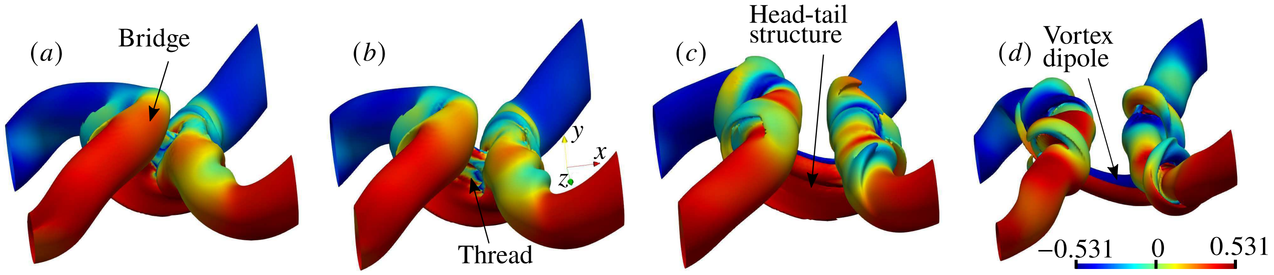

Figure 4. A closer look at the viscous vortex reconnection process in Fig. 3 at different times (a) t = 55; (b) t = 57; (c) t = 65 and (d) t = 80.

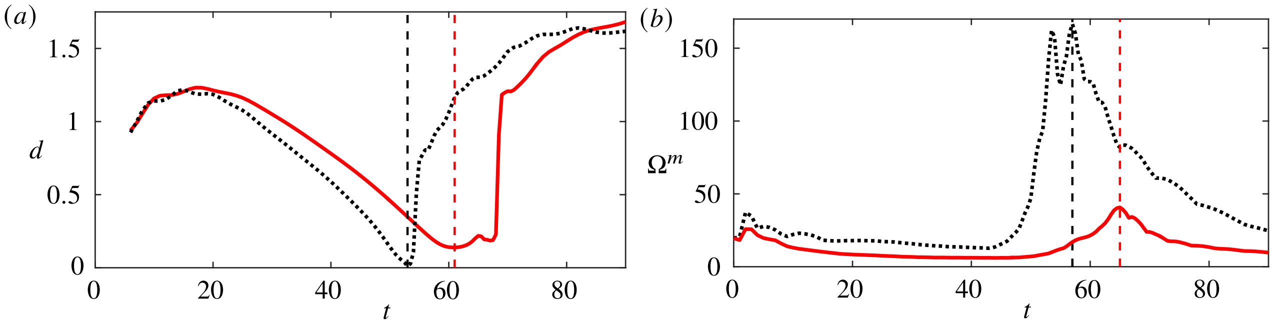

Figure 5. Time evolution of (*a*) separation distance and (*b*) maximum enstrophy for the cases $\mathrm{H_W}1$ (• • • • • •) and $\mathrm{H_W}2$ (———). The vertical dashed lines denote minimum separation distance at $t = 53$ ($\mathrm{H_W}1$) and $t = 61$ ($\mathrm{H_W}2$) in (*a*), while in (*b*) they denote local peaks at $t = 57$ ($\mathrm{H_W}1$) and $t = 65$ ($\mathrm{H_W}2$).

vorticity regions to convect faster, leading to the formation of a head-tail structure (see Fig. 4*c*), where the head part forms a vortex dipole, while the tail gets dissipated due to viscosity (see Fig. 4*d*). However, unlike antiparallel line vortices, in cases $\mathrm{H_W}1$ and $\mathrm{H_W}2$, the reconnection plane actually moves towards the inflow plane due to the self-induced velocity of the hairpin tip (see Figs. 3*a* and 3*d*). In fact, Melander & Hussain (1988) divided this whole process into three stages: (I) inviscid advection, (II) bridging and (III) threading, all of which are clearly visible in Figs. 3 and 4.

The evolution of the hairpin at $Re = 1500$ (case $\mathrm{H_W}2$ of Table 1) is identical to that of the higher Reynolds number case $\mathrm{H_W}1$, except the onset of the reconnection process getting delayed and its duration extended, which can be observed from the evolution of separation distance d and maximum enstrophy Ω^m, shown in Fig. 5. For finding d, the vortex centre tracking method using vortex lines is used (see Yao & Hussain, 2020*c*), where a single vortex line is injected from the vorticity centroid of the hairpin leg at $z > 0$, such that it traces the entire hairpin vortex. This yields the minimum distance between the hairpin legs before reconnection, while after reconnection two vortex lines are needed to find the separation distance: one of which is injected from the inflow plane and the other from the vorticity centroid of the vortex ring core in $z = 0$ plane.

At the lower Re (case $\mathrm{H_W}2$), the reconnection is delayed and thus both the separation distance attaining its minimum (see Fig. 5*a*) and the maximum enstrophy reaching its local peak happen at later times (see Fig. 5*b*). Note that the value of Ω^m peaks after reconnection due to the formation of small-scale structures (Hussain & Duraisamy, 2011; Yao & Hussain, 2020*b*), while in Fig. 5(*b*), multiple peaks in Ω^m at $Re = 3000$ are visible, whereas for $Re = 1500$, a single peak is seen. In fact, the number of such peaks and their magnitudes increases with Re, which is important in determining whether a finite time singularity (FTS) is possible for the Navier-Stokes equations (see Beale *et al.*, 1984; Fefferman, 2006). We briefly note that the theoretical model of Moffatt & Kimura (2019*b*) predicted the presence of a physical, but not a mathematical singularity, while the DNS results of Yao & Hussain (2020*a*) showed that even a physical singularity is impossible, even though its occurrence in the inviscid limit is unknown yet.

As expected, increased viscosity also leads to thicker vortex cores and slower movements of the reconnection plane towards the inflow (see for case $\mathrm{H_W}2$), but the three stages of reconnection identified by Melander & Hussain (1988) remains identical. For even higher Reynolds numbers ($Re > 3000$), the bridges move away faster, leading to threads that cut and reconnect, while the tail portion of the head-tail structure become unstable via Kelvin-Helmholtz instability, rolling up into multiple dipoles. These head dipoles undergo further reconnections leading to the formation of vortex rings, hairpin packets and several small-scale structures (Yao & Hussain, 2020*b*; Mcgavin & Pontin, 2018; Beardsell *et al.*, 2016; Hussain & Duraisamy, 2011).

Effects of background flows

In Figs. 6 and 7, we compare the cases with background flows with the case in quiescent fluid, all at $Re = 1500$, via the changes in different parameters due to the inclusion of background flows. The isosurfaces of vorticity magnitude in Fig. 6 clearly show the hairpin vortex to get convected along with the corresponding background flow, increasing the lengths of hairpin legs, more so for the case with a higher convection velocity (see case $\mathrm{H_U}1$ of Fig. 6*a*), as expected. Similarly, the case with positive shear (case $\mathrm{H_S}1$ of Fig. 6*c*) convects the hairpin more than that with negative shear (case $\mathrm{H_S}2$ of Fig. 6*d*), as in the former the hairpin moves into higher velocity regions of the background flow as time progresses. In general, the background stream opposes the self-induced motions of the hairpin tip, carrying the tip along with it. Note that Fig. 6 also shows the onset of a second reconnection process upstream of the first, indicating the occurrence of a sequence of such

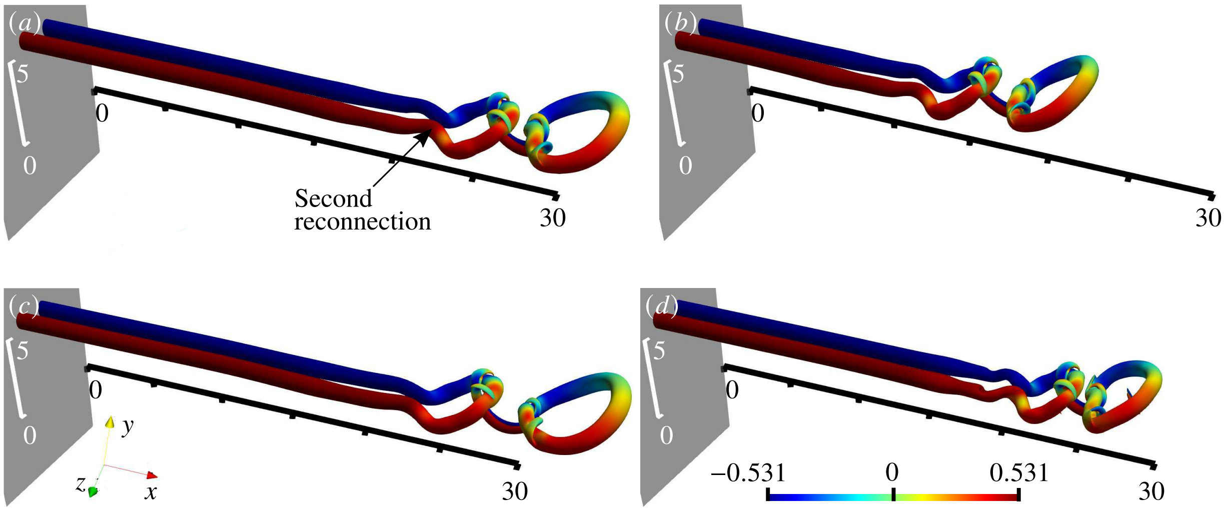

Figure 6. Isosurfaces of vorticity magnitude $|\omega| = 0.15|\omega|_0$ coloured with contours of ω_x for the cases H_U1 (*a*), H_U2 (*b*), H_S1 (*c*) and H_S2 (*d*) at $t = 85$. The rest are same as figure 3.

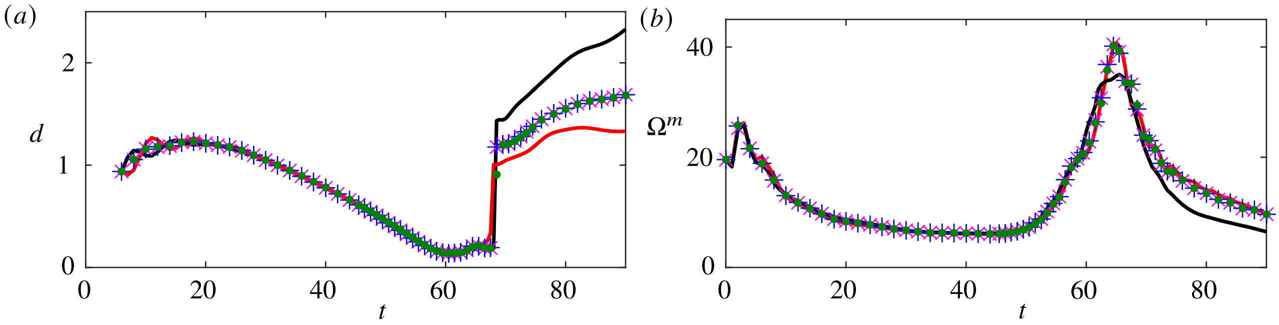

Figure 7. Time evolution of (*a*) separation distance and (*b*) maximum enstrophy for the cases H_W2 (●), H_U1 (×), H_U2 (+), H_S1 (——) and H_S2 (——). The minimum d occurs at $t = 60.5$ (H_U1, H_U2), $t = 61$ (H_W2, H_S2) and $t = 61.5$ (H_S1), while the local peak in Ω^m occur at $t = 65$ (H_W2, H_U1, H_U2, H_S2) and $t = 65.5$ (H_S1).

reconnections as the hairpin is convected by the background flow.

As shown in Fig. 7*a*, the time evolution of separation distances for all the cases at $Re = 1500$ studied here (including the quiescent case H_W2) are largely similar before the reconnection event, except for the slight earlier occurence of the distance minimum for the uniformly convecting flow cases of H_U1 and H_U2. Further, uniform convection yields an insignificant effect on the evolution of Ω^m and its peak value (see Fig. 7*b*). Note that to compare with the H_W2 case, the corresponding background flows are first subtracted before calculating enstrophy for the other cases. Hence, it may be inferred that the uniform convection of background stream does not alter the reconnection process in any way, except for the convection of reconnection plane downstream, thereby reconfirming the local nature of this process as is also reported in the literature.

In contrast to the uniformly convecting flow cases, once uniform background shear is applied, although it still has a rather small effect on d during the initial vorticity rearrangement phases, but such a flow significantly alters the dynamics post reconnection, as is visible in Fig. 7(*a*). This different evolution after reconnection occurs as different parts of vortex structures, especially the vortex rings, experience different background flow velocities, manifested via varying distances between the secondary hairpin and vortex ring in Fig. 6. The corresponding reconnection time obtained by fitting the linear portion of d before reconnection indicated slight delayed onset of the process for cases H_S1 and H_S2, when compared to the uniformly convecting cases. On comparing the shear cases, the local peak of Ω^m and the minimum of d occurs later for H_S1, indicating a delayed onset of reconnection, while for H_S2, they occur earlier at the same time as that of H_W2. At this stage, the reason for such differences is not clear and more simulations with different background flows and Reynolds numbers are being carried out, whose findings will be reported in the future.

SUMMARY

The main findings of this work are summarised in the following.

1. The evolution of an isolated hairpin vortex in a quiescent fluid is identical to the Biot-Savart evolution of the vortex line till pinch-off (see Moin *et al.*, 1986). The initial hairpin gets split into a secondary hairpin and vortex ring due to the viscous vortex reconnection process, as observed with the present hairpin configuration, which is also identical to other configurations reported in the literature, especially antiparallel line vortices (Yao & Hussain, 2020*b*).
2. A decrease in Reynolds number leads to a delay in the onset of reconnection and an increase in the duration of this process.

3. The addition of a background flow leads to the increase in length of hairpin legs due to the convection of hairpin tip with the flow. The uniformly convecting flows do not alter the reconnection process. In contrast, positive and negative shear accelerates and decelerates, respectively, the onset of reconnection.

Partial funding from the Office of Naval Research Global (ONRG) NICOP grant with award number N62909-17-1-2131 with Dr. S. Ahmed as the Project Monitor is gratefully acknowledged. For computing resources, we acknowledge the use of the "SahasraT" Cray XC40 system at the Supercomputer Education and Research Centre (SERC) of the Indian Institute of Science for most of our simulations.

REFERENCES

Archer, P. J., Thomas, T. G. & Coleman, G. N. 2008 Direct numerical simulation of vortex ring evolution from the laminar to the early turbulent regime. *J. Fluid Mech.* **598**, 201–226.

Balakrishna, N., Mathew, J. & Samanta, A. 2020 Inviscid and viscous global stability of vortex rings. *J. Fluid Mech.* **902**.

Beale, J. T., Kato, T. & Majda, A. 1984 Remarks on the breakdown of smooth solutions for the 3-d Euler equations. *Commun. Math. Phys.* **94** (1), 61–66.

Beardsell, G., Dufresne, L. & Dumas, G. 2016 Investigation of the viscous reconnection phenomenon of two vortex tubes through spectral simulations. *Phys. Fluids* **28** (9), 095103.

De Waele, A. T. A. M. & Aarts, R. G. K. M. 1994 Route to vortex reconnection. *Phys. Rev. Lett.* **72** (4), 482.

Fefferman, C. L. 2006 Existence and smoothness of the Navier-Stokes equation. In *The Millennium Prize Problems*, pp. 57–70. American Mathematical Society.

Fukumoto, Y. & Hattori, Y. 2005 Curvature instability of a vortex ring. *J. Fluid Mech.* **526**, 77–115.

Hama, F. R. 1962 Progressive deformation of a curved vortex filament by its own induction. *Phys. Fluids* **5** (10), 1156–1162.

Hussain, F. & Duraisamy, K. 2011 Mechanics of viscous vortex reconnection. *Phys. Fluids* **23** (2), 021701.

Laizet, S. & Lamballais, E. 2009 High-order compact schemes for incompressible flows: A simple and efficient method with quasi-spectral accuracy. *J. Comput. Phys.* **228** (16), 5989–6015.

Laizet, S. & Li, N. 2011 Incompact3d: A powerful tool to tackle turbulence problems with up to o (105) computational cores. *Int. J. Numer. Methods Fluids* **67** (11), 1735–1757.

Mcgavin, P. & Pontin, D. I. 2018 Vortex line topology during vortex tube reconnection. *Phys. Rev. Fluids* **3** (5), 054701.

Melander, M. V. & Hussain, F. 1988 Cut-and-connect of two antiparallel vortex tubes. In *Studying Turbulence Using Numerical Simulation Databases*, , vol. 2, pp. 257–286. Center for Turbulence Research.

Michalke, A. 1984 Survey on jet instability theory. *Progress in Aerospace Sciences* **21**, 159–199.

Moffatt, H. K. & Kimura, Y. 2019*a* Towards a finite-time singularity of the navier–stokes equations part 1. derivation and analysis of dynamical system. *J. Fluid Mech.* **861**, 930–967.

Moffatt, H. K. & Kimura, Y. 2019*b* Towards a finite-time singularity of the navier–stokes equations. part 2. vortex reconnection and singularity evasion. *J. Fluid Mech.* **870**.

Moin, P., Leonard, A. & Kim, J. 1986 Evolution of a curved vortex filament into a vortex ring. *Phys. Fluids* **29** (4), 955–963.

Naveen, B. 2022 On late stages of transition in round jets. PhD thesis, Indian Institute of Science.

Widnall, S. E. & Tsai, C. Y. 1977 The instability of the thin vortex ring of constant vorticity. *Philos. Trans. Royal Soc. A* **287** (1344), 273–305.

Yao, J. & Hussain, F. 2020*a* On singularity formation via viscous vortex reconnection. *J. Fluid Mech.* **888**.

Yao, J. & Hussain, F. 2020*b* A physical model of turbulence cascade via vortex reconnection sequence and avalanche. *J. Fluid Mech.* **883**.

Yao, J. & Hussain, F. 2020*c* Separation scaling for viscous vortex reconnection. *J. Fluid Mech.* **900**, R4.